

<https://helda.helsinki.fi>

---

## Martini 3 : a general purpose force field for coarse-grained molecular dynamics

Souza, Paulo C. T.

2021-04

---

Souza , P C T , Alessandri , R , Barnoud , J , Thallmair , S , Faustino , I , Grunewald , F , Patmanidis , I , Abdizadeh , H , Bruininks , B M H , Wassenaar , T A , Kroon , P C , Melcr , J , Nieto , V , Corradi , V , Khan , H M , Domanski , J , Javanainen , M , Martinez-Seara , H , Reuter , N , Best , R B , Vattulainen , I , Monticelli , L , Periole , X , Tieleman , D P , de Vries , A H & Marrink , S J 2021 , ' Martini 3 : a general purpose force field for coarse-grained molecular dynamics ' , Nature methods , vol. 18 , no. 4 , pp. 382-+ . <https://doi.org/10.1038/s41592-021-01098-3>

---

<http://hdl.handle.net/10138/334681>

<https://doi.org/10.1038/s41592-021-01098-3>

---

unspecified

acceptedVersion

---

*Downloaded from Helda, University of Helsinki institutional repository.*

*This is an electronic reprint of the original article.*

*This reprint may differ from the original in pagination and typographic detail.*

*Please cite the original version.*

# Martini 3: A General Purpose Force Field for Coarse-Grained Molecular Dynamics

Paulo C. T. Souza<sup>\*1,2</sup>, Riccardo Alessandri<sup>1</sup>, Jonathan Barnoud<sup>1,3</sup>, Sebastian Thallmair<sup>1,4</sup>, Ignacio Faustino<sup>1</sup>, Fabian Grunewald<sup>1</sup>, Ilias Patmanidis<sup>1</sup>, Haleh Abdizadeh<sup>1</sup>, Bart M.H. Bruininks<sup>1</sup>, Tsjerk A. Wassenaar<sup>1</sup>, Peter C. Kroon<sup>1</sup>, Josef Melcr<sup>1</sup>, Vincent Nieto<sup>2</sup>, Valentina Corradi<sup>5</sup>, Hanif M. Khan<sup>5,6</sup>, Jan Domański<sup>7,8</sup>, Matti Javanainen<sup>9,10</sup>, Hector Martinez-Seara<sup>9</sup>, Nathalie Reuter<sup>6</sup>, Robert B. Best<sup>8</sup>, Ilpo Vattulainen<sup>10,11</sup>, Luca Monticelli<sup>2</sup>, Xavier Periole<sup>12,13</sup>, D. Peter Tieleman<sup>5</sup>, Alex H. de Vries<sup>1</sup>, Siewert J. Marrink<sup>\*1</sup>

<sup>1</sup> Groningen Biomolecular Sciences and Biotechnology Institute and Zernike Institute for Advanced Material, University of Groningen, Nijenborgh 7, 9747 AG Groningen, The Netherlands.

<sup>2</sup> Molecular Microbiology and Structural Biochemistry, UMR 5086 CNRS & University of Lyon, 7 Passage du Vercors, F-69367, Lyon, France.

<sup>3</sup> Intangible Realities Laboratory, University of Bristol, School of Chemistry, Cantock's Close, Bristol BS8 1TS, United Kingdom.

<sup>4</sup> Frankfurt Institute for Advanced Studies, Ruth-Moufang-Str. 1, 60438 Frankfurt am Main, Germany.

<sup>5</sup> Centre for Molecular Simulation and Department of Biological Sciences, University of Calgary, 2500 University Drive NW, Calgary, Alberta T2N 1N4, Canada.

<sup>6</sup> Department of Chemistry and Computational Biology Unit, University of Bergen, N-5020 Bergen, Norway.

<sup>7</sup> Department of Biochemistry, University of Oxford, South Parks Road, Oxford OX1 3QU, United Kingdom.

<sup>8</sup> Laboratory of Chemical Physics, National Institute of Diabetes and Digestive and Kidney Diseases, National Institutes of Health, Bethesda, Maryland 20892-0520, United States.

<sup>9</sup> Institute of Organic Chemistry and Biochemistry, Czech Academy of Sciences, CZ-16610 Prague 6, Czech Republic.

<sup>10</sup> Computational Physics Laboratory, Tampere University, FI-33100 Tampere, Finland.

<sup>11</sup> Department of Physics, University of Helsinki, FI-00014 Helsinki, Finland.

<sup>12</sup> Department of Chemistry, Aarhus University, Aarhus C, Denmark.

<sup>13</sup> School of Biological Sciences, The University of Auckland, Symonds Street 3A, Auckland, New Zealand.

\* Corresponding authors: Paulo C. T. Souza – paulocts@gmail.com  
Siewert J. Marrink – s.j.marrink@rug.nl

## 54 **ABSTRACT**

55 The coarse-grained Martini force field is widely used in biomolecular  
56 simulations. Here, we present the refined model, Martini 3 (<http://cgmartini.nl>),  
57 with an improved interaction balance, new bead types, and expanded ability  
58 to include specific interactions representing, e.g. hydrogen bonding and  
59 electronic polarizability. The new model allows more accurate predictions of  
60 molecular packing and interactions in general, which is exemplified with a vast  
61 and diverse set of applications, ranging from oil/water partitioning and  
62 miscibility data to complex molecular systems, involving protein-protein and  
63 protein-lipid interactions and material science applications as ionic liquids and  
64 aedamers.

## 65 **INTRODUCTION**

67 The molecular dynamics (MD) simulation technique has become an  
68 indispensable tool in natural sciences, offering a spatio-temporal resolution  
69 unmatched by any experimental technique<sup>1</sup>. A major bottleneck of MD is the  
70 limited time and length scales that are accessible. To overcome this limitation,  
71 coarse-grained (CG) models representing groups of atoms by effective beads,  
72 have achieved widespread use<sup>2</sup>. The Martini model is among the most  
73 popular CG models in the field of biomolecular simulation, due to its easy-to-  
74 use building block principle. Martini relies on a four-to-one mapping scheme  
75 (i.e., on average four heavy atoms and associated hydrogens are mapped  
76 into one CG bead), and has been parametrized using a top-down approach  
77 with thermodynamic partitioning data as the main target<sup>3,4</sup>. Non-bonded  
78 interactions between neutral beads of Martini are solely described by

79 Lennard-Jones (LJ) potentials, while charged beads also include Coulombic  
80 interactions. The interaction strength of the LJ potential (i.e. its well depth) is  
81 used to discriminate between different levels of polarity of the CG beads. The  
82 model features four main classes of CG bead types, denoted C, N, P, and Q  
83 representing non-polar, intermediately polar, polar, and charged chemical  
84 groups, respectively<sup>4</sup>. Sub-labels are used to make a further distinction within  
85 a class in terms of degree of polarity or hydrogen donor/acceptor capabilities.  
86 In principle, all beads have the same size, denoted as regular (R) beads. By  
87 way of exception, special small (S) beads were introduced to model ring-like  
88 compounds for which a four-to-one mapping scheme is inadequate<sup>4</sup>. To  
89 reproduce correct stacking and hydrogen bonding distances between  
90 nucleotides, even smaller tiny (T) beads were found necessary<sup>5</sup>.  
91 Parametrization of the cross-interactions between S- and T-beads with R-  
92 beads, however, was done on an *ad-hoc* basis.

93 The Martini force field is used in a wide range of applications in diverse fields  
94 including structural biology<sup>6-8</sup>, biophysics<sup>9,10</sup>, biomedicine<sup>11</sup>,  
95 nanotechnology<sup>12,13</sup>, and materials design<sup>14,15</sup>. With its growing use, however,  
96 a number of shortcomings of the Martini model have recently been identified.  
97 One of the most important problems is the observation that certain molecules  
98 tend to interact too strongly. This has been reported for proteins and  
99 carbohydrates in solution, as well as for membrane embedded proteins<sup>16-18</sup>.  
100 The origin lies among others in small but systematic deviations in packing and  
101 intermolecular interactions<sup>19</sup>. Besides, the coverage of chemical space for  
102 broader applications was uneven, and in some cases, such as selectivity of  
103 nucleobase pairing<sup>5,20</sup>, consistency was difficult to obtain given the limited



104 bead types and sizes. To alleviate these problems, we undertook a re-  
105 balancing of all non-bonded interaction terms of the Martini model, including  
106 the addition of new beads and labels. The new version, called Martini 3,  
107 enables more accurate simulations of molecular systems in general. In this  
108 paper, we present the key features of Martini 3 combined with examples of  
109 new applications and improvements in relation to the previous Martini model.

110

## 111 **RESULTS**

112 **Re-parametrization of the beads.** In Martini 3, the new parametrization  
113 strategy was based on the construction of prototype models of polar and non-  
114 polar molecules in all three Martini resolutions. Self- (R-R, S-S, and T-T) and  
115 cross-interactions (R-S, R-T, and S-T) of the different bead sizes were  
116 optimized to be well-balanced (**Supplementary Notes, sections B1 and B2**).  
117 In terms of chemical types, the beads were separated into three blocks:  
118 organic, ions, and water (**Supplementary Notes, section A1**). The organic  
119 (containing P-, N-, and C-beads) and ion (Q-beads) blocks have been  
120 subjected to independent parametrizations, where different trends in self-  
121 interaction, solvation, and transfer free energy upon bead size change were  
122 included (**Supplementary Notes, sections A1, B2, and B3**). In contrast to  
123 the previous version, water is defined as a separate bead type (called W),  
124 which enables optimization of water properties independently from other  
125 targets; for example, the freezing of water at room temperature (a problem  
126 sometimes encountered with the previous water model) no longer occurs. In  
127 addition, it is available in three different sizes as well (**Supplementary Notes,**  
128 **section B4**). Together with this optimization strategy, the new Martini 3 model

129 also features a fully revised interaction matrix (**Supplementary Notes,**  
130 **section A2**) and new intermediate interaction levels, added to smoothen the  
131 transition between chemical types (**Supplementary Notes, section A3**).  
132 Bead assignment and validation of the models were not only based on  
133 experimental transfer free energies, but also included solvent miscibility data  
134 (**Supplementary Notes, sections A6 and C2, and Supplementary Results,**  
135 **sections E4-E6**) and a series of benchmark tests, ranging from structural  
136 properties of bilayers to dimerization potentials of mean force (PMFs) of  
137 proteins (**Methods, section 3, Supplementary Notes, section B5 and**  
138 **Supplementary Results, sections F1-F5**).

139 The improved interaction balance between regular and smaller bead types is  
140 illustrated by the close to ideal mixing behavior of pure solvents composed of  
141 molecules mapped at different resolutions (**Fig. 1A**). Integration of radial  
142 distribution functions, defined as Kirkwood–Buff integrals ( $G_{ij}$ ), are used here  
143 to quantify the degree of miscibility of the multi-resolution liquid water model  
144 (**Fig. 1B**). Theoretically, pair differences in Kirkwood–Buff integrals ( $\Delta G_{ij}$ )  
145 should be equal to zero for all  $i,j$  pairs in ideal mixtures<sup>21,22</sup> while real mixtures  
146 that closely approach ideal behavior (like benzene-toluene) show values  
147 around  $\pm 1 \text{ cm}^3/\text{mol}^{22}$ . Our multi-resolution water model shows  $\Delta G_{ij} \approx -0.3$   
148  $\text{cm}^3/\text{mol}$ , indicating that the balance achieved with the new parametrization  
149 closely captures an ideal mixing behavior.

150 The accuracy of CG models containing ring or branched fragments, which rely  
151 heavily on smaller bead types, is also greatly increased in Martini 3. For  
152 example, the binary mixing behavior of various solvents (**Supplementary**  
153 **Results, sections E4-E6**) and the transfer free energies of many linear,

154 branched, and ring-like compounds (**Fig 1C** and **Supplementary Results,**  
155 **section E1**) are now in very good agreement with experimental data. The  
156 mean absolute error of transfer free energies compared to the experimental  
157 data is 2 kJ/mol, with 86% of the molecules presenting errors lower than 3  
158 kJ/mol.

159 Another benefit of the recalibrated interactions is the disappearance of the  
160 artificially large desolvation free energy barriers that contribute to slow  
161 dissociation processes of the previous Martini 2 models. The problem, that  
162 was initially observed in dimerization of nucleobases<sup>5,19</sup>, is thus solved, as  
163 highlighted by the comparison of Martini 2 and Martini 3 PMFs between  
164 cytosine and guanine (left panel of **Fig. 1D**). Note that there is room for further  
165 improvement, as the free energy minima of the CG PMF profiles with Martini 3  
166 are shifted relative to the all-atom profiles because the bead sizes  
167 representing nitrogen-containing groups are not optimal to reproduce  
168 hydrogen bonding distances. In addition, the difference between C-G and G-G  
169 base pairs is not as large as in the atomistic case (~20 kJ/mol). However, it is  
170 still large enough (~8 kJ/mol) to provide specificity.

171 The proper balancing of R-, S-, and T-beads in Martini 3 also implies that the  
172 mapping choice of an arbitrary molecule to its Martini representation is now  
173 better defined. S- and T-beads are not only suited to represent ring-like  
174 compounds, but also used for cases involving 3-to-1 and 2-to-1 mapping of  
175 linear and branched chemical groups (**Supplementary Notes, section C1**).

176

177 **Covering the chemical space with new beads and labels.** Together with a  
178 thorough revision of the interaction strengths, in Martini 3, we extend the  
179 number of chemical bead types and the ability to modify the bead properties  
180 depending on the chemical details of the underlying moieties. Each P-, N-,  
181 and C-class now has 6 bead types with different degrees of polarity, which  
182 enables a more precise definition of different chemical groups by assigning  
183 them to certain bead types. Additionally, we introduce a new X-class of beads  
184 to model halo-compounds (**Supplementary Notes, section A1**). In the  
185 previous version of Martini, some of the bead types were already sub-  
186 classified according to their ability to act as hydrogen bond donor, acceptor, or  
187 both. This property can be now attributed to all bead types of intermediate or  
188 polar nature (N- or P- class). The effective interaction strength between donor  
189 and acceptor pairs is increased, whereas donor-donor and acceptor-acceptor  
190 pairs are weakened (**Supplementary Notes, section A4**). For example,  
191 Martini 3 correctly reproduces the trends in hydrogen bond-based pairing of  
192 nucleobases<sup>5,20</sup> without the use of special-purpose beads specifically for  
193 nucleobases (right panel of **Fig. 1D**). Note that chemical groups that can act  
194 as both donor and acceptor at the same time are always represented by the  
195 pure beads of the P- and N-class in Martini 3.

196 Next to the fine-tuning based on hydrogen bonding capabilities, we introduce  
197 the possibility to change the interactions based on the electronic polarizability.  
198 Depending on inductive or conjugate effects caused by chemical  
199 functionalization, non-polar molecules can be polarized, i.e., they can acquire  
200 an electron-donor (or “enriched”, label “e”) or electron-acceptor (or “vacancy”,  
201 label “v”) character, which can promote preferential interactions. Polarizable

groups in Martini 3 can be distinguished through the label “e/v” which can only be applied to the C- and X-class. A nice example of their application is the strong and specific interaction between electron donor and electron acceptor aromatic rings in aedamers, a class of molecules that have been studied extensively in the context of biomimetic folding and self-assembly<sup>23,24</sup>. The use of “e/v” allows Martini 3 to capture the preferential interaction between 1,5-dialkoxynaphthalene (DAN) and naphthalene diimide (NDI) (left panel of **Fig. 2A**) experimentally observed via NMR titration<sup>23</sup> and atomistic simulation data. Self-assembly of amide-linked tetramers shows preferential formation of alternating stacks of DAN and NDI, which is also measured by NMR and isothermal titration calorimetry investigations<sup>24</sup>. On top of hydrogen bonding and electron polarization labels, all beads can have their self-interaction fine-tuned by other sub-labels (as further described in the **Supplementary Notes, section A4**).

Chemical groups carrying monovalent charges +1/-1 are represented in Martini by the class of Q-beads (**Supplementary Notes, section A1**). The original Martini model only considers monovalent ions, and was solely optimized for regular bead sizes which represented small ions and their first hydration shell. In Martini 3, charged groups can have either R-, S-, or T-size. The tiny size category allows modeling of small, bare ions, enabling applications that involve ion binding where (part of) the hydration shell is lost. This feature is exemplified by the binding of sodium ions (represented by a charged tiny bead) to a buried small cavity localized in the core of the adenosine A<sub>2A</sub> receptor (**Fig. 2B**). X-ray crystallographic<sup>25</sup> and ligand binding assays<sup>26</sup> confirm the importance of sodium ions for the structure and for the

227 allosteric modulation of the A<sub>2A</sub> receptor. Note that an extensive validation of  
 228 the lipid models in Martini 3 was performed to allow simulations of  
 229 transmembrane and peripheral membrane proteins (see **Supplementary**  
 230 **Results, section F1**).

231 In addition to the smaller sizes, the Q-class was also expanded to five bead  
 232 types, following the classical Hofmeister series trend<sup>27,28</sup> (**Supplementary**  
 233 **Notes, section B3 and Supplementary Results, section F2**). At one  
 234 extreme, the Q5 bead may be used to represent hard monovalent ions with  
 235 the smallest polarizability, e.g. inorganic ions such as R<sub>2</sub>PO<sub>4</sub><sup>-</sup>. At the other  
 236 end of the Martini Hofmeister series, the Q1 type models polarizable soft  
 237 monovalent ions, like N(CH<sub>3</sub>)<sub>4</sub><sup>+</sup>, and implicitly includes in the LJ potential ion-π  
 238 interactions. Such differences in behavior of the different Q-bead types are  
 239 exemplified by MD simulations of the anion transfer between aqueous  
 240 solutions and organophosphonium-based ionic liquids (**Fig. 2C and**  
 241 **Supplementary Results, section F2**). Harder ions such as Cl<sup>-</sup> (modeled as  
 242 TQ5 with -1 charge) tend to stay in the water phase, together with Na<sup>+</sup> ions  
 243 (TQ5<sup>+</sup> bead). In contrast, softer ions like ClO<sub>4</sub><sup>-</sup> (Q2<sup>-</sup> bead) can exchange with  
 244 Br<sup>-</sup> (SQ4<sup>-</sup> bead) or (partially) PF<sub>6</sub><sup>-</sup> (Q1<sup>-</sup> bead) from the ionic liquid phase. In the  
 245 case of the biphasic system using trihexyltetradecylphosphonium bromide  
 246 ([P<sub>66614</sub>][Br]), direct comparison to experimental data shows good agreement  
 247 for the anion transfer trends<sup>28,29</sup>. The new Q-bead types also impact  
 248 biologically relevant systems, as exemplified by preferential cation-π  
 249 interaction between choline groups (Q1<sup>+</sup> bead) of phosphatidylcholine lipids  
 250 and aromatic residues of the *Bacillus thuringiensis* phosphatidylinositol-  
 251 specific phospholipase C (*Bt*PI-PLC). In the previous version, such specific

252 interaction between soft ions and aromatic molecules were solely included in  
253 the recently updated polarizable Martini implementation<sup>30</sup>. However, in Martini  
254 3, the different Q-bead types allow easier (implicit) incorporation of such  
255 interactions without the need for additional partial charges.

256 On top of the new chemical types, all Q-beads can use the hydrogen-bonding  
257 labels (called in this case “p/n”). They represent organic charged molecules or  
258 fragments, such as  $\text{R-CH}_2\text{-COO}^-$  and  $\text{R-CH}_2\text{-NH}_3^+$ , and also introduce  
259 modifications in the Hofmeister trends of the pure Q-beads (**Supplementary**  
260 **Notes, section A4**). Positively charged hydrogen donors (“p” label) interact  
261 more strongly with non-polar beads, as expected in cation- $\pi$  interactions. On  
262 the other hand, negatively charged hydrogen acceptors (“n” label), have  
263 stronger interactions with neutral polar beads, mimicking the stronger  
264 hydrogen-bonds with anions. To complete the ion block, we explicitly include  
265 a new D-bead for divalent ions (such as  $\text{Ca}^{2+}$ ), which are typically hard ions.

266

267 **Improving packing and protein-protein interactions.** Another change in  
268 philosophy with respect to the previous Martini models is the definition of  
269 bonded interactions. Instead of using the center of mass of the mapped  
270 chemical groups to define the geometry of the molecule, we now use a size-  
271 shape concept aimed at preserving the volume of molecules in comparison to  
272 all-atom reference structures. This choice and the proper use of Martini 3  
273 bead sizes (**Supplementary Notes, sections C1 and C2**) lead to more  
274 realistic molecular packing. As a consequence, the hydration of protein  
275 pockets and channels is improved, as illustrated by the Fragaceatoxin C  
276 (FraC) nanopore inserted in a lipid bilayer (**Fig. 3A**). The pore of FraC

277 remains open over the whole trajectory in Martini 3, as indicated by X-ray  
278 crystallography<sup>31</sup> and electro-osmotic flow assays<sup>32</sup>, while in Martini 2 it is  
279 closed.

280 Another example of accurate packing is the stacking predictions of thiophene  
281 derivatives in bulk heterojunction solar cells composed of poly(3-hexyl-  
282 thiophene) (P3HT) and phenyl-C61-butyric acid methyl ester (PCBM) (**Fig.**  
283 **3B**). The morphology of these organic solar cells is a determinant for high-  
284 efficiency devices<sup>33</sup>. The scattering profiles computed with Martini 3 show  
285 improved agreement with Martini 3 in relation to P3HT lamellar (peak around  
286  $q \approx 0.45 \text{ \AA}^{-1}$ ) and stacking ( $q \approx 1.65 \text{ \AA}^{-1}$ ) experimental distances<sup>33,34</sup>.

287 The use of bonds based on molecular volume and the appropriate choice of  
288 chemical bead types, sizes, and labels also controls the interaction density of  
289 the model, which has an important impact on the strength of collective  
290 interactions between molecules<sup>19</sup>. In order to test to what extent the changes  
291 in non-bonded and bonded interactions reduce the over-estimated  
292 aggregation of proteins, we performed extensive simulations comprised of  
293 solutions of soluble proteins as well as membrane embedded proteins. These  
294 systems were simulated under conditions in which proteins do not aggregate  
295 and, preferentially, stay as monomers. For soluble proteins (**Fig. 3C**),  
296 qualitative tests were performed with the headpiece domain of chicken villin<sup>35</sup>,  
297 and the modified and mutated cellulose-binding domain from *Cellulomonas*  
298 *fimi* (EXG-CBM), which is an example of a protein completely free of charged  
299 side chains that can maintain solubility, stability, and function<sup>36</sup>. Trends are  
300 well-captured in Martini 3, with both proteins mainly staying as monomers in  
301 pure water (with only counter-ions to neutralize the system in the case of



302 villin). The villin headpiece showed salting-in behavior (i.e. less aggregation)  
303 under addition of 0.4M of NaCl, which was also observed for certain soluble  
304 proteins at low ionic strengths<sup>37</sup>. On the other hand, EXG-CBM only showed  
305 salting-out behavior (i.e. more aggregation), which was expected based on  
306 experimental data<sup>36</sup>. In contrast, both proteins aggregate in Martini 2, forming  
307 a single and stable aggregate during the simulation.

308 Polyleucine (K<sub>2</sub>-L<sub>26</sub>-K<sub>2</sub>) was selected to evaluate the aggregation propensity in  
309 membranes. Experimental evidence with this transmembrane (TM) protein  
310 model indicates a preference for the monomeric state in a bilayer  
311 environment<sup>38–40</sup>. Both Martini 2 and 3 show that the hydrophobic mismatch  
312 between TM length and membrane thickness can play a role in the  
313 aggregation, with Martini 3 showing a higher percentage of the monomeric  
314 state (**Fig. 3D**). To quantitatively evaluate the strength of protein-protein  
315 interactions in a membrane environment, we also considered the dimerization  
316 of four selected transmembrane (TM) helices: the TM domains of the receptor  
317 tyrosine kinases EphA1 and ErbB1; the red blood cell protein glycophorin A  
318 (GpA); as well as the well-known model peptide WALP23 (left panel of **Fig.**  
319 **3E**). For EphA1 and ErbB1, experimental dimerization free energies in a  
320 membrane environment have been estimated using Förster resonance energy  
321 transfer (FRET)<sup>41,42</sup>. For GpA, dimerization free energies range from around -  
322 15 kJ/mol (in various cell membrane environments)<sup>43,44</sup> to -31.5 kJ/mol  
323 (GALLEX assay in *E. coli* inner membranes)<sup>45,46</sup> or -50.6 kJ/mol (steric trap in  
324 POPC bilayers)<sup>47</sup>. WALP peptides have been characterized thoroughly during  
325 the past two decades, including their self-association<sup>48</sup>. For each one of the  
326 four peptide dimers, we compared experimental dimerization free energies

327 with the free energies predicted by the Martini 2 and Martini 3 model  
328 predictions. Martini 3 shows not only to be able to capture the correct trends,  
329 but also to quantitatively reproduce the experimental affinities. The binding  
330 mode also becomes improved as highlighted for GpA (right panel of **Fig. 3E**).  
331 The GpA homodimer structure with Martini 3 closely resembles experimental  
332 results obtained with NMR spectroscopy and crystallography<sup>49–51</sup>.

333 In summary, for both soluble and transmembrane proteins, we observed that  
334 the Martini 3 models are in much better agreement with experimental data  
335 than before. Another advantage of the current Martini 3 protein model is that  
336 the default bead type representing the protein backbone in Martini 3 (a regular  
337 P2 bead) no longer depends on the secondary structure. In addition, the  
338 representation of protein flexibility can now be improved by the use of Gō-like  
339 models<sup>52</sup>.

340

## 341 **DISCUSSION**

342 In this paper we have described the new version of the Martini force field,  
343 which shows numerous improvements in relation to the previous version.  
344 However, inherent limitations to the process of coarse-graining, related to  
345 transferability and representability problems<sup>53–55</sup> are still part of the model. An  
346 important drawback is the limited structural detail, that is a consequence of  
347 representing multiple atoms with isotropic interaction sites. This is most  
348 noticeable for the Martini water model, which represents four water molecules  
349 with a single LJ site and will certainly not capture any of the higher order  
350 structural correlations of real water. The role of explicit water in a CG model

351 such as Martini is mostly to provide a good solvent for polar compounds  
352 resulting in realistic partitioning. For applications requiring finer details,  
353 structure-based CG models are more suitable<sup>56,57</sup>. Another fundamental  
354 limitation is the entropy-enthalpy compensation. The loss of internal degrees  
355 of freedom for groups of atoms represented by a CG bead inevitably reduces  
356 the entropy of the system. Since the Martini force field is based on  
357 reproducing free energies, this requires a concomitant reduction in the  
358 enthalpy. As consequence, inaccurate entropy-enthalpy balance affects the  
359 temperature dependence of several properties and reduces the transferability  
360 to different state points. To probe transferability, we performed temperature  
361 dependent calculations for a number of solvent systems as well as lipid  
362 membranes (**Supplementary Results F**). Temperature dependent properties,  
363 like the heat expansion coefficient and heat capacity of water and n-octane,  
364 are very well captured by Martini 3, but this is not true for the hydrophobic  
365 effect, that shows the opposite trend with respect to atomistic models, in line  
366 with previous findings<sup>58</sup>. Note that the use of higher-resolution S- or T-  
367 particles does not remedy this problem, as these bead types were  
368 parameterized mainly to be compatible with the regular (R-type) beads and  
369 should be used primarily to represent parts of the system that cannot be  
370 adequately mapped with R-particles. Potential improvements with respect to  
371 the temperature transferability of our model could make use of environment  
372 dependent potentials<sup>59</sup> or CG beads with embedded sites, such as the  
373 polarizable water models<sup>60,61</sup>, where incorporation of quadrupole moment  
374 might be required<sup>58</sup>. Bottom-up CG models that are derived with minimization  
375 of the information loss<sup>54</sup> as parameterization target might also perform better.

376 For a more in depth discussion of these and related issues with respect to the  
377 Martini coarse-graining philosophy, we refer to previous papers<sup>62,63</sup>.  
378 Keeping these limitations in mind, Martini 3 offers a versatile and easy to use  
379 generic force field to simulate molecular processes at a semi-quantitative level  
380 of accuracy. In relation to the previous model, the excessive over-estimated  
381 aggregation<sup>19</sup> is substantially reduced. We expect that Martini 3 will allow for  
382 more realistic predictions of protein interactions, as well as more accurate  
383 simulations of molecular systems in general. The increased number of bead  
384 types and interaction levels makes the model even more versatile, covering a  
385 larger part of chemical space with appropriate building blocks. Based on this  
386 new foundation, further optimizations for different classes of molecules are  
387 currently ongoing, including the use of Gō-potentials to alleviate limitations of  
388 protein conformational flexibility, a re-optimization of the bonded potentials of  
389 lipids and other biomolecular classes, as well as a compatible polarizable  
390 water model for applications requiring more realistic screening of electrostatic  
391 interactions. Finally, we foresee new application horizons for the Martini  
392 model in the field of materials science<sup>64,65</sup> and high-throughput drug design<sup>66</sup>.

393

#### 394 **ONLINE CONTENT**

395 Methods, including statements of data and code availability, supplementary  
396 information, and any other associated content and references, are available in  
397 the online version of the paper at <https://doi.org/10.1038/sXXXXX-XXX-XXXX->  
398 X.

399

## 400    **ACKNOWLEDGMENTS**

401    We thank all members of the S.J.M. group and also external users for testing  
402    Martini 3 in its open-beta version. In particular, we would like to thank C.F.E.  
403    Schroer, P.W.J.M. Frederix, W. Pezeshkian, M.N. Melo, H.I. Ingólfsson, M.  
404    Tsanai, M. König, P. A. Vainikka, T. Zijp, L. Gaifas, J.H. van der Woude, M.  
405    Espinoza Cangahuala, M. Scharte, J. Cruiming, L.M. van der Sleen, V.  
406    Verduijn, A.H. Beck Frederiksen, B. Schiøtt, M. Sikora, P. Schmalhorst, K.  
407    Pluhackova, C. Arnarez, C.A. López, E. Jefferys, and M.S.P. Sansom for their  
408    preliminary tests with a lot of different systems including aedamers, sugars,  
409    amino acids, deep eutectic solvents, lipids, peptides, and proteins. We also  
410    thank the Center for Information Technology of the University of Groningen for  
411    providing access to the Peregrine high-performance computing cluster. We  
412    acknowledge the National Computing Facilities Foundation (NCF) of The  
413    Netherlands Organization for Scientific Research (NWO), CSC – IT Center for  
414    Science Ltd (Espoo, Finland), and CINES (France) for providing computing  
415    time. Work in the S.J.M. group was supported by an ERC Advanced Grant  
416    “COMP-MICR-CROW-MEM”. R.A. thanks The Netherlands Organisation for  
417    Scientific Research NWO (Graduate Programme Advanced Materials, No.  
418    022.005.006) for financial support. L.M. acknowledges the Institut National de  
419    la Santé et de la Recherche Medicale (INSERM) and the Agence Nationale  
420    de la Recherche (ANR) for funding (grant no. ANR-17-CE11-0003) and  
421    GENCI-CINES for computing time (grant no. A0060710138). S.T.  
422    acknowledges the support from the European Commission via a Marie  
423    Skłodowska-Curie Actions individual fellowship (MicroMod-PSII, grant  
424    agreement 748895). M.J. thanks the Emil Aaltonen foundation for financial

425 support. I.V. thanks the Academy of Finland (Center of Excellence program  
426 (grant no. 307415)), Sigrid Juselius Foundation, the Helsinki Institute of Life  
427 Science fellow program, and the HFSP (research grant Ref.-No:  
428 RGP0059/2019). R.B. and J.D. were supported by the intramural research  
429 program of the NIDDK, NIH. Their work utilized the computational resources  
430 of the NIH HPC Biowulf cluster. (<http://hpc.nih.gov>). H.M.-S. acknowledges  
431 the Czech Science Foundation (19-19561S). J.B. acknowledges funding from  
432 the TOP grant of S.J.M. (NWO) and the EPSRC program grant  
433 EP/P021123/1. Work in D.P.T.'s group is supported by the Natural Sciences  
434 and Engineering Research Council (Canada) and Compute Canada, funded  
435 by the Canada Foundation for Innovation. D.P.T. acknowledges further  
436 support from the Canada Research Chairs program.

437

## 438 **AUTHOR CONTRIBUTIONS**

439 P.C.T.S. and S.J.M. conceived the project with suggestions from R.A., A.H.V.,  
440 J.B., and S.T.; P.C.T.S. generated and optimized all bead parameters;  
441 P.C.T.S., R.A., and J.B. generated the topology and bonded parameters of all  
442 CG models with suggestions from S.T. and I.F.; P.C.T.S., R.A., A.H.V., and  
443 F.G. performed the simulations and analysis involving transfer free energies,  
444 solvent and polymer properties; P.C.T.S., S.T., J.B., and J.M. performed the  
445 simulations and analysis involving lipid bilayers; P.C.T.S., I.F., and R.A.  
446 performed the simulations and analysis involving nucleobases; P.C.T.S., I.P.,  
447 and A.H.V. generated the models, performed the simulations and analysis  
448 involving aedamers; P.C.T.S., and F.G. generated the models, performed the  
449 simulations and analysis involving ionic liquids and ionic water solutions; R.A.

450 generated the models, performed the simulations and analysis involving bulk  
451 heterojunctions, with suggestions from L.M. regarding the fullerene model;  
452 P.C.T.S., J.B., H.A., R.A., B.M.H.B., S.T., J.M., V.N., X.P., M.J., H.M.K., J.D.,  
453 V.C., and H.M.-S. performed the simulations and analysis involving amino  
454 acids, peptides and proteins; J.B., T.W., P.K., and S.T. developed some tools  
455 and scripts used to generate the CG models and to run the MD simulations;  
456 L.M., R.B., P.T., N.R., I.V., A.H.V., and S.J.M. provided guidance and  
457 supervision in the studies performed by their respective group members and  
458 collaborators; P.C.T.S. and S.J.M. wrote the main manuscript, with  
459 contributions from all the authors; P.C.T.S. prepared the figures with  
460 contributions from R.A., B.M.H.B., H.M.K., and A.H.V.; P.C.T.S. wrote the  
461 Methods with contributions from all the authors. P.C.T.S. wrote the  
462 Supplementary Information, with contributions from all the authors. All the  
463 authors revised and approved the final version of the manuscript, Online  
464 Methods, and Supplementary Information.

465

## 466 **COMPETING INTERESTS**

467 The authors declare no competing interests.

468

## 469 **REFERENCES**

- 470 1. Bottaro, S. & Lindorff-Larsen, K. Biophysical experiments and biomolecular  
471 simulations: A perfect match? *Science* **361**, 355–360 (2018).
- 472 2. Ingólfsson, H. I. *et al.* The power of coarse graining in biomolecular  
473 simulations. *Wiley Interdiscip. Rev. Comput. Mol. Sci.* **4**, 225–248 (2014).

- 474 3. Marrink, S. J., De Vries, A. H. & Mark, A. E. Coarse Grained Model for  
475 Semiquantitative Lipid Simulations. *J. Phys. Chem. B* **108**, 750–760 (2004).
- 476 4. Marrink, S. J., Risselada, H. J., Yefimov, S., Tieleman, D. P. & de Vries, A.  
477 H. The MARTINI force field: coarse grained model for biomolecular  
478 simulations. *J. Phys. Chem. B* **111**, 7812–7824 (2007).
- 479 5. Uusitalo, J. J., Ingólfsson, H. I., Akhshi, P., Tieleman, D. P. & Marrink, S. J.  
480 Martini Coarse-Grained Force Field: Extension to DNA. *J. Chem. Theory*  
481 *Comput.* **11**, 3932–3945 (2015).
- 482 6. Abellón-Ruiz, J. *et al.* Structural basis for maintenance of bacterial outer  
483 membrane lipid asymmetry. *Nat. Microbiol.* **2**, 1616–1623 (2017).
- 484 7. Yen, H. Y. *et al.* PtdIns(4,5)P2 stabilizes active states of GPCRs and  
485 enhances selectivity of G-protein coupling. *Nature* **559**, 423–427 (2018).
- 486 8. Van Eerden, F. J., Melo, M. N., Frederix, P. W. J. M., Periole, X. & Marrink,  
487 S. J. Exchange pathways of plastoquinone and plastoquinol in the  
488 photosystem II complex. *Nat. Commun.* **8**, 15214 (2017).
- 489 9. Vögele, M., Köfinger, J. & Hummer, G. Hydrodynamics of Diffusion in Lipid  
490 Membrane Simulations. *Phys. Rev. Lett.* **120**, (2018).
- 491 10. Agostino, M. D., Risselada, H. J., Lürick, A., Ungermann, C. & Mayer, A. A  
492 tethering complex drives the terminal stage of SNARE-dependent membrane  
493 fusion. *Nature* **551**, 634–638 (2017).
- 494 11. Jeena, M. T. *et al.* Mitochondria localization induced self-assembly of  
495 peptide amphiphiles for cellular dysfunction. *Nat. Commun.* **8**, 26 (2017).
- 496 12. Jiang, Z. *et al.* Subnanometre ligand-shell asymmetry leads to Janus-like  
497 nanoparticle membranes. *Nat. Mater.* **14**, 912–917 (2015).



- 498 13. Maingi, V. *et al.* Stability and dynamics of membrane-spanning DNA  
499 nanopores. *Nat. Commun.* **8**, 14784 (2017).
- 500 14. Frederix, P. W. J. M. *et al.* Exploring the sequence space for (tri-)peptide  
501 self-assembly to design and discover new hydrogels. *Nat. Chem.* **7**, 30–37  
502 (2015).
- 503 15. Bochicchio, D., Salvalaglio, M. & Pavan, G. M. Into the dynamics of a  
504 supramolecular polymer at submolecular resolution. *Nat. Commun.* **8**, 147  
505 (2017).
- 506 16. Stark, A. C., Andrews, C. T. & Elcock, A. H. Toward optimized potential  
507 functions for protein-protein interactions in aqueous solutions: osmotic second  
508 virial coefficient calculations using the MARTINI coarse-grained force field. *J.*  
509 *Chem. Theory Comput.* **9**, 4176–4185 (2013).
- 510 17. Javanainen, M., Martinez-Seara, H. & Vattulainen, I. Excessive  
511 aggregation of membrane proteins in the Martini model. *PLoS One* **12**,  
512 e0187936 (2017).
- 513 18. Schmalhorst, P. S., Deluweit, F., Scherrers, R., Heisenberg, C.-P. &  
514 Sikora, M. Overcoming the Limitations of the MARTINI Force Field in  
515 Simulations of Polysaccharides. *J. Chem. Theory Comput.* **13**, 5039–5053  
516 (2017).
- 517 19. Alessandri, R. *et al.* Pitfalls of the Martini Model. *J. Chem. Theory*  
518 *Comput.* **15**, 5448–5460 (2019).
- 519 20. Uusitalo, J. J., Ingólfsson, H. I., Marrink, S. J. & Faustino, I. Martini  
520 Coarse-Grained Force Field: Extension to RNA. *Biophys. J.* **113**, 246–256  
521 (2017).

- 522 21. Ben-Naim, A. *Molecular theory of solutions*. (Oxford University Press,  
523 2006).
- 524 22. Ploetz, E. A., Benteñitis, N. & Smith, P. E. Kirkwood-Buff integrals for ideal  
525 solutions. *J. Chem. Phys.* **132**, 164501 (2010).
- 526 23. Zych, A. J. & Iverson, B. L. Synthesis and Conformational  
527 Characterization of Tethered, Self-Complexing 1,5-  
528 Dialkoxynaphthalene/1,4,5,8-Naphthalenetetracarboxylic Diimide Systems. *J.*  
529 *Am. Chem. Soc.* **122**, 8898–8909 (2000).
- 530 24. Gabriel, G. J. & Iverson, B. L. Aromatic oligomers that form hetero  
531 duplexes in aqueous solution. *J. Am. Chem. Soc.* **124**, 15174–15175 (2002).
- 532 25. Liu, W. *et al.* Structural basis for allosteric regulation of GPCRs by sodium  
533 ions. *Science* **337**, 232–236 (2012).
- 534 26. Gao, Z. G. & Ijzerman, A. P. Allosteric modulation of A(2A) adenosine  
535 receptors by amiloride analogues and sodium ions. *Biochem. Pharmacol.* **60**,  
536 669–676 (2000).
- 537 27. Okur, H. I. *et al.* Beyond the Hofmeister Series: Ion-Specific Effects on  
538 Proteins and Their Biological Functions. *J. Phys. Chem. B* **121**, 1997–2014  
539 (2017).
- 540 28. Dupont, D., Depuydt, D. & Binnemans, K. Overview of the Effect of Salts  
541 on Biphasic Ionic Liquid/Water Solvent Extraction Systems: Anion Exchange,  
542 Mutual Solubility, and Thermomorphic Properties. *J. Phys. Chem. B* **119**,  
543 6747–6757 (2015).
- 544 29. Naert, P., Rabaey, K. & Stevens, C. V. Ionic liquid ion exchange:  
545 Exclusion from strong interactions condemns cations to the most weakly

546 interacting anions and dictates reaction equilibrium. *Green Chem.* **20**, 4277–  
547 4286 (2018).

548 30. Khan, H. M. *et al.* Capturing Choline-Aromatics Cation- $\pi$ Interactions in the  
549 MARTINI Force Field. *J. Chem. Theory Comput.* **16**, 2550–2560 (2020).

550 31. Tanaka, K., Caaveiro, J. M. M., Morante, K., González-Manãs, J. M. &  
551 Tsumoto, K. Structural basis for self-assembly of a cytolytic pore lined by  
552 protein and lipid. *Nat. Commun.* **6**, 6337 (2015).

553 32. Huang, G., Willems, K., Soskine, M., Wloka, C. & Maglia, G. Electro-  
554 osmotic capture and ionic discrimination of peptide and protein biomarkers  
555 with FraC nanopores. *Nat. Commun.* **8**, 935 (2017).

556 33. Alessandri, R., Uusitalo, J. J., De Vries, A. H., Havenith, R. W. A. &  
557 Marrink, S. J. Bulk Heterojunction Morphologies with Atomistic Resolution  
558 from Coarse-Grain Solvent Evaporation Simulations. *J. Am. Chem. Soc.* **139**,  
559 3697–3705 (2017).

560 34. Chiu, M. Y., Jeng, U. S., Su, C. H., Liang, K. S. & Wei, K. H. Simultaneous  
561 use of small- and wide-angle X-ray techniques to analyze nanometerscale  
562 phase separation in polymer heterojunction solar cells. *Adv. Mater.* **20**, 2573–  
563 2578 (2008).

564 35. Petrov, D. & Zagrovic, B. Are Current Atomistic Force Fields Accurate  
565 Enough to Study Proteins in Crowded Environments? *PLoS Comput. Biol.* **10**,  
566 e1003638 (2014).

567 36. Højgaard, C. *et al.* A Soluble, Folded Protein without Charged Amino Acid  
568 Residues. *Biochemistry* **55**, 3949–3956 (2016).

- 569 37. Ruckenstein, E. & Shulgin, I. L. Effect of salts and organic additives on the  
570 solubility of proteins in aqueous solutions. *Advances in Colloid and Interface*  
571 *Science* **123–126**, 97–103 (2006).
- 572 38. Zhou, F. X., Cocco, M. J., Russ, W. P., Brunger, A. T. & Engelman, D. M.  
573 Interhelical hydrogen bonding drives strong interactions in membrane  
574 proteins. *Nat. Struct. Biol.* **7**, 154–160 (2000).
- 575 39. Zhou, F. X., Merianos, H. J., Brunger, A. T. & Engelman, D. M. Polar  
576 residues drive association of polyleucine transmembrane helices. *Proc. Natl.*  
577 *Acad. Sci. U. S. A.* **98**, 2250–2255 (2001).
- 578 40. Grau, B. *et al.* The role of hydrophobic matching on transmembrane helix  
579 packing in cells. *Cell Stress* **1**, 90–106 (2017).
- 580 41. Chen, L., Merzlyakov, M., Cohen, T., Shai, Y. & Hristova, K. Energetics of  
581 ErbB1 transmembrane domain dimerization in lipid bilayers. *Biophys. J.* **96**,  
582 4622–4630 (2009).
- 583 42. Artemenko, E. O., Egorova, N. S., Arseniev, A. S. & Feofanov, A. V.  
584 Transmembrane domain of EphA1 receptor forms dimers in membrane-like  
585 environment. *Biochim. Biophys. Acta* **1778**, 2361–7 (2008).
- 586 43. Sarabipour, S. & Hristova, K. Glycophorin A transmembrane domain  
587 dimerization in plasma membrane vesicles derived from CHO, HEK 293T, and  
588 A431 cells. *Biochim. Biophys. Acta - Biomembr.* **1828**, 1829–1833 (2013).
- 589 44. Chen, L., Novicky, L., Merzlyakov, M., Hristov, T. & Hristova, K.  
590 Measuring the Energetics of Membrane Protein Dimerization in Mammalian  
591 Membranes. *J. Am. Chem. Soc.* **132**, 3628–3635 (2010).

592 45. Nash, A., Notman, R. & Dixon, A. M. De novo design of transmembrane  
 593 helix-helix interactions and measurement of stability in a biological membrane.  
 594 *Biochim. Biophys. Acta - Biomembr.* **1848**, 1248–1257 (2015).

595 46. Finger, C. *et al.* The Stability of Transmembrane Helix Interactions  
 596 Measured in a Biological Membrane. *J. Mol. Biol.* **358**, 1221–1228 (2006).

597 47. Hong, H., Blois, T. M., Cao, Z. & Bowie, J. U. Method to measure strong  
 598 protein-protein interactions in lipid bilayers using a steric trap. *Proc. Natl.*  
 599 *Acad. Sci. U. S. A.* **107**, 19802–19807 (2010).

600 48. Sparr, E. *et al.* Self-association of transmembrane  $\alpha$ -helices in model  
 601 membranes: Importance of helix orientation and role of hydrophobic  
 602 mismatch. *J. Biol. Chem.* **280**, 39324–39331 (2005).

603 49. MacKenzie, K. R., Prestegard, J. H. & Engelman, D. M. Transmembrane  
 604 helix dimer: Structure and implications. *Science (80-. )*. **276**, 131–133 (1997).

605 50. Trenker, R., Call, M. E. & Call, M. J. Crystal Structure of the Glycophorin A  
 606 Transmembrane Dimer in Lipidic Cubic Phase. *J. Am. Chem. Soc.* **137**,  
 607 15676–15679 (2015).

608 51. Domański, J., Sansom, M. S. P., Stansfeld, P. J. & Best, R. B. Balancing  
 609 Force Field Protein–Lipid Interactions To Capture Transmembrane Helix–  
 610 Helix Association. *J. Chem. Theory Comput.* **14**, 1706–1715 (2018).

611 52. Souza, P. C. T., Thallmair, S., Marrink, S. J. & Mera-Adasme, R. An  
 612 Allosteric Pathway in Copper, Zinc Superoxide Dismutase Unravels the  
 613 Molecular Mechanism of the G93A Amyotrophic Lateral Sclerosis-Linked  
 614 Mutation. *J. Phys. Chem. Lett.* **10**, 7740–7744 (2019).

615 53. Brini, E. *et al.* Systematic coarse-graining methods for soft matter  
 616 simulations-a review. *Soft Matter* **9**, 2108–2119 (2013).

617 54. Foley, T. T., Shell, M. S. & Noid, W. G. The impact of resolution upon  
 618 entropy and information in coarse-grained models. *J. Chem. Phys.* **143**,  
 619 243104 (2015).

620 55. Wagner, J. W., Dama, J. F., Durumeric, A. E. P. & Voth, G. A. On the  
 621 representability problem and the physical meaning of coarse-grained models.  
 622 *J. Chem. Phys.* **145**, 044108 (2016).

623 56. Wörner, S. J., Bereau, T., Kremer, K. & Rudzinski, J. F. Direct route to  
 624 reproducing pair distribution functions with coarse-grained models via  
 625 transformed atomistic cross correlations. *J. Chem. Phys.* **151**, 244110 (2019).

626 57. Noid, W. G., Chu, J. W., Ayton, G. S. & Voth, G. A. Multiscale coarse-  
 627 graining and structural correlations: Connections to liquid-state theory. *J.*  
 628 *Phys. Chem. B* **111**, 4116–4127 (2007).

629 58. Wu, Z., Cui, Q. & Yethiraj, A. Driving force for the association of  
 630 hydrophobic peptides: The importance of electrostatic interactions in coarse-  
 631 grained water models. *J. Phys. Chem. Lett.* **2**, 1794–1798 (2011).

632 59. Jin, J., Yu, A. & Voth, G. A. Temperature and Phase Transferable Bottom-  
 633 up Coarse-Grained Models. *J. Chem. Theory Comput.* (2020).  
 634 doi:10.1021/acs.jctc.0c00832

635 60. Yesylevskyy, S. O., Schäfer, L. V, Sengupta, D. & Marrink, S. J.  
 636 Polarizable water model for the coarse-grained MARTINI force field. *PLoS*  
 637 *Comput. Biol.* **6**, e1000810 (2010).

638 61. Michalowsky, J., Schäfer, L. V., Holm, C. & Smiatek, J. A refined  
 639 polarizable water model for the coarse-grained MARTINI force field with long-  
 640 range electrostatic interactions. *J. Chem. Phys.* **146**, 054501 (2017).

- 641 62. Marrink, S. J. & Tieleman, D. P. Perspective on the Martini model. *Chem.*  
642 *Soc. Rev.* **42**, 6801–22 (2013).
- 643 63. Bruininks, B. M. H., Souza, P. C. T. & Marrink, S. J. A Practical View of  
644 the Martini Force Field. in *Methods in Molecular Biology* **2022**, 105–127  
645 (Humana Press Inc., 2019).
- 646 64. Liu, J. *et al.* Enhancing Molecular n-Type Doping of Donor-Acceptor  
647 Copolymers by Tailoring Side Chains. *Adv. Mater.* **30**, 1704630 (2018).
- 648 65. Vazquez-Salazar, L. I., Selle, M., de Vries, A., Marrink, S. J. & Souza, P.  
649 C. T. Martini coarse-grained models of imidazolium-based ionic liquids: from  
650 nanostructural organization to liquid-liquid extraction. *Green Chem.* **22**, 7376–  
651 7386 (2020).
- 652 66. Souza, P. C. T. *et al.* Protein–ligand binding with the coarse-grained  
653 Martini model. *Nat. Commun.* **11**, 1–11 (2020).

## FIGURE LEGENDS

**Figure 1: Rebalancing R-, S-, and T-beads** – (A) Snapshots of simulation boxes containing mixtures of dodecane and water in three resolutions. (B) Radial distribution functions ( $g_{ij}$ ) for all bead combinations in the multi-resolution mixture of water. (C) Water-oil transfer free energies ( $\Delta G$ ) computed for around 260 data points using Martini 3. (D) Hydrogen bonding potential of mean force (PMF) between nucleobases. On the left, comparison between Martini 2 and 3 for the cytosine-guanine base pair. On the right, comparison of the cytosine-guanine (C-G) and guanine-guanine (G-G) base pairs using Martini 3. In both plots, CHARMM and AMBER atomistic data are also reported<sup>5</sup> for comparison. Errors are estimated with bootstrapping and displayed as transparent shades. In the case of Martini, errors are smaller than 0.1 kJ/mol, and hence are not visible in the graphs.

**Figure 2: New chemical bead types, sub-labels, and applications** – (A) Self-assembly of aedamers. The left panel shows the dimerization free energies ( $\Delta G_{\text{dim}}$ ) of pegylated monomers of 1,5-dialkoxynaphthalene (DAN) and naphthalene diimide (NDI). Errors are estimated with bootstrapping. The right panel shows the self-assembled duplex dimer formed by amide-linked tetramers of NDI (green) and DAN (orange). (B) As indicated by X-ray crystallography<sup>25</sup>, sodium ions (charged TQ5 bead) can bind to a buried small cavity in the core of the adenosine  $A_{2A}$  receptor. (C) Charged Q-beads in Martini 3 follow the classical Hofmeister series, as exemplified by the anion transfer between salt aqueous solutions and organophosphonium-based ionic liquids (right panel). Errors in the average anion transfer percentage are estimated by block averaging. (D) Preferential cation- $\pi$  interaction between choline groups (Q1 bead) of phosphatidylcholine lipids and aromatic residues of the *Bacillus thuringiensis* phosphatidylinositol-specific phospholipase C (*BtPI-PLC*). The depth of insertion of each amino acid of *BtPI-PLC* is in very good agreement with the insertion obtained from an atomistic MD simulation<sup>30</sup>.



**Figure 3: Improving packing, cavities and reducing protein stickiness – (A)** Hydration of  
 Fragaceatoxin C (FraC) nanopore inserted in a lipid bilayer. **(B)** Scattering profiles and a  
 Martini 3 snapshot of a bulk heterojunction morphology of poly(3-hexyl-thiophene) (P3HT, in  
 red) and phenyl-C61-butyric acid methyl ester (PCBM, in blue) formed after solvent  
 evaporation and annealing simulations.  $I(q)$  corresponds to scattering intensity and  $q$  is the  
 reciprocal space vector. **(C)** Aggregation levels of the soluble proteins villin headpiece and  
 the modified EXG-CBM in different salt concentrations. **(D)** Aggregation levels of polyleucine  
 helices in POPC and DLPC bilayers. Errors in the average monomer percentage of **(C)** and  
**(D)** are estimated by block averaging. **(E)** Dimerization of transmembrane helices. Left panel  
 shows a comparison between experimental and calculated values for the mole fraction  
 standard Gibbs free energy of dimerization ( $\Delta G_{ass}^X$ ) of the following transmembrane protein  
 domains: ErbB1, EphA1, WALP23 and GpA. Simulation errors are estimated with  
 bootstrapping while experimental data was obtained in the literature<sup>41-48</sup>. In the case of GpA,  
 error was estimated by the mean absolute error of four independent experimental data<sup>43-47</sup>. A  
 comparison between experimental and simulated binding modes of GpA is highlighted in the  
 right panel. The experimental structure was taken from solution NMR in micelles (PDB code  
 AFO)<sup>49</sup>. Near identical experimental structures were obtained by ssNMR in nanodiscs and X-  
 ray crystallography in a lipid cubic phase<sup>49-51</sup>.

700  
 701

## 702 **ONLINE METHODS**

703

### 704 **1) CG models**

705 CG mappings of small molecules were initially inspired by the standard Martini  
706 2 models, when they were available. Due to the well-balanced properties of  
707 the regular (R), small (S), and tiny (T) beads in Martini 3, the CG models now  
708 follow more specific rules for mapping. For instance, over-representing 3-to-1  
709 or 2-to-1 fragments by the usage of R-beads is always avoided. Aromatic  
710 rings without substituents are composed of T-beads and, in case of  
711 substituents, S-beads are used. Aliphatic rings without substituents are  
712 usually based on S-beads, which better reproduce their molecular shape.  
713 More technical details about the mapping rules and bead types used are  
714 given in the **Supplementary Notes, sections C1 and C3**. As in the previous  
715 version of Martini<sup>5,20,67–69</sup>, bonded parameters are based on atomistic  
716 simulations or high-resolution experimental data. The main difference in  
717 Martini 3 lies in the protocol to derive bond lengths, which are now based on  
718 matching overall volume and shape of the molecules (**Supplementary Notes,**  
719 **section C2**). In this spirit, the bonded parameters of the protein models were  
720 also slightly modified from the standard Martini 2.2 values<sup>68,70</sup>, including the  
721 addition of side chain corrections<sup>71</sup>, based on experimental reference  
722 structures. Backbone bead types do not depend on the secondary structure  
723 anymore, but are now represented by P2 beads, except for proline (SP1a),  
724 alanine (SP2, with an additional bead for the side chain) and glycine (SP1).  
725 Adapted versions of Gō-like models<sup>72</sup> or Elastic Networks<sup>73</sup> were used to  
726 maintain the tertiary protein structure. All CG protein models were constructed  
727 using *Martinize2*, described in **Supplementary Codes, section H1**. Lipid

mapping was inspired by the previous Martini model<sup>74–77</sup>, but now following the Martini 3 rules for mapping and also with adaptations in the bonded parameters inspired by the “extensible model” of Carpenter *et al.*<sup>78</sup>.

## 2) General setup for CG MD simulations and Analysis

Settings for the CG simulations followed, in general, the “new” Martini set of simulation parameters<sup>79</sup> using the leap-frog algorithm<sup>80</sup> for integrating the equations of motion. The Verlet neighbor search algorithm<sup>81</sup> is used to update the neighbor list every 20 steps with a buffer tolerance of 0.005 kJ·mol<sup>-1</sup>·ps<sup>-1</sup>. For the Lennard-Jones terms, we used a cutoff scheme with a value of 1.1 nm and the Verlet cutoff scheme<sup>82</sup> for the potential-shift. Long range electrostatic interactions were treated with reaction field<sup>83</sup> or Particle Mesh Ewald (PME)<sup>84</sup>, with relative permittivity set to  $\epsilon_r=15$  and a cutoff value of 1.1 nm. Reaction field was used for most of the systems, except the ones explicitly mentioning PME. Periodic boundary conditions were used in all three dimensions. For the production simulations, the velocity rescaling thermostat<sup>85</sup> (coupling time constant of 1.0 ps) and the Parrinello-Rahman barostat<sup>86</sup> (coupling time constant of 12.0 ps) were employed to maintain temperature and pressure, respectively. Except for equilibration runs, a time step of 20 fs was used for all systems. CG simulation settings are available as input files for GROMACS on the Martini portal <http://cgmartini.nl>. GROMACS 2016.x and 2018.x were used to run all the MD simulations<sup>87,88</sup>. For automated running and managing the Martini 3 simulations, we provide an updated version of *Martinate*<sup>89,90</sup>, described in **Supplementary Codes, section H2**. All the analysis were performed using *gmx analysis tools* (GROMACS 2016 and 2018)<sup>87,88</sup>, VMD

753 1.9.4a12<sup>91</sup>, xmgrace (5.1.25) and MDAnalysis<sup>92</sup>. The graphs were plotted  
754 using Excel 2016, xmgrace (5.1.25) and gnuplot (5.2). Figures were compiled  
755 using VMD 1.9.4a12 and Inkscape 1.1.

756

### 757 **3) Parameter calibration, tests and validation**

758 In order to parametrize the LJ parameters of single beads and also test the  
759 Martini 3 CG models, many molecular systems and methods were used in this  
760 work. The overall iterative approach was not based in rigorous separation of  
761 calibration and validation groups. As Martini is based on pair interactions, it is  
762 hard to find simple systems that cover enough points in the interaction matrix  
763 for all bead size combinations. So, complex systems are not only used for  
764 validation but can be part of the calibration. The tests performed were  
765 separated in “tiers”, which represent systems with different level of complexity.  
766 In “tier 0”, isolate beads and simple-molecules are mainly used for calibration  
767 of LJ parameters, with balance of different bead sizes and thermodynamics  
768 data (e.g. liquid-liquid partitioning and miscibility) used as main targets. In the  
769 intermediate “tier 1”, bilayer properties are checked, together with qualitative  
770 tests, applied to systems like soluble and transmembrane proteins. These  
771 qualitative tests are designed as “yes-or-no” questions to evaluate the overall  
772 quality of the force field. At the same time, some points in the interaction  
773 matrix were also tested and fine-tuned here. In the final “tier 2”, quantitative  
774 tests involving complex systems are performed, including comparisons with  
775 experimental or atomistic simulation data. Here most of the system are  
776 considered validation. For a complete overview of the parametrization  
777 strategy used, see the **Supplementary Notes, section B**. The

778 **Supplementary Notes, section D** provide details of the specific systems and  
779 methods used in the tests performed to parametrize and validate the new  
780 Martini 3 LJ parameters. Further information on research design is available in  
781 the Life Sciences Reporting Summary linked to this article.

782

#### 783 **DATA AVAILABILITY**

784 Force-field parameters and procedures (e.g. tutorials) are publicly available at  
785 <http://cgmartini.nl>. Simulation Data (e.g. trajectories) supporting the results of  
786 this paper are available from the corresponding authors upon reasonable  
787 request.

788

#### 789 **CODE AVAILABILITY**

790 *Martinize2* (for which the manuscript is in preparation) and *Martinate* codes  
791 used in this work are publicly available at <https://github.com/marrink-lab/>. For  
792 a more detailed information, see **Supplementary Codes, section H**.

793

794

795

## 796 REFERENCES

- 797 67. López, C. A. *et al.* Martini Coarse-Grained Force Field: Extension to  
798 Carbohydrates. *J. Chem. Theory Comput.* **5**, 3195–3210 (2009).
- 799 68. Monticelli, L. *et al.* The MARTINI Coarse-Grained Force Field: Extension  
800 to Proteins. *J. Chem. Theory Comput.* **4**, 819–834 (2008).
- 801 69. Grunewald, F., Rossi, G., de Vries, A. H., Marrink, S. J. & Monticelli, L.  
802 Transferable MARTINI Model of Poly(ethylene Oxide). *J. Phys. Chem. B* **122**,  
803 7436–7449 (2018).
- 804 70. de Jong, D. H. *et al.* Improved Parameters for the Martini Coarse-Grained  
805 Protein Force Field. *J. Chem. Theory Comput.* **9**, 687–97 (2013).
- 806 71. Herzog, F. A., Braun, L., Schoen, I. & Vogel, V. Improved Side Chain  
807 Dynamics in MARTINI Simulations of Protein–Lipid Interfaces. *J. Chem.*  
808 *Theory Comput.* **12**, 2446–2458 (2016).
- 809 72. Poma, A. B., Cieplak, M. & Theodorakis, P. E. Combining the MARTINI  
810 and Structure-Based Coarse-Grained Approaches for the Molecular Dynamics  
811 Studies of Conformational Transitions in Proteins. *J. Chem. Theory Comput.*  
812 **13**, 1366–1374 (2017).
- 813 73. Periole, X., Cavalli, M., Marrink, S.-J. & Ceruso, M. A. Combining an  
814 Elastic Network With a Coarse-Grained Molecular Force Field: Structure,  
815 Dynamics, and Intermolecular Recognition. *J. Chem. Theory Comput.* **5**,  
816 2531–2543 (2009).
- 817 74. Marrink, S. J., Risselada, H. J., Yefimov, S., Tieleman, D. P. & de Vries,  
818 A. H. The MARTINI force field: coarse grained model for biomolecular  
819 simulations. *J. Phys. Chem. B* **111**, 7812–7824 (2007).

820 75. Wassenaar, T. A., Ingólfsson, H. I., Böckmann, R. A., Tieleman, D. P. &  
821 Marrink, S. J. Computational Lipidomics with *insane*: A Versatile Tool for  
822 Generating Custom Membranes for Molecular Simulations. *J. Chem. Theory*  
823 *Comput.* **11**, 2144–2155 (2015).

824 76. Melo, M. N., Ingólfsson, H. I. & Marrink, S. J. Parameters for Martini  
825 sterols and hopanoids based on a virtual-site description. *J. Chem. Phys.* **143**,  
826 243152 (2015).

827 77. López, C. A., Sovova, Z., van Eerden, F. J., de Vries, A. H. & Marrink, S.  
828 J. Martini Force Field Parameters for Glycolipids. *J. Chem. Theory Comput.* **9**,  
829 1694–1708 (2013).

830 78. Carpenter, T. S. *et al.* Capturing Phase Behavior of Ternary Lipid Mixtures  
831 with a Refined Martini Coarse-Grained Force Field. *J. Chem. Theory Comput.*  
832 **14**, 6050–6062 (2018).

833 79. de Jong, D. H., Baoukina, S., Ingólfsson, H. I. & Marrink, S. J. Martini  
834 straight: Boosting performance using a shorter cutoff and GPUs. *Comput.*  
835 *Phys. Commun.* **199**, 1–7 (2016).

836 80. Hockney, R. W., Goel, S. P. & Eastwood, J. W. Quiet high-resolution  
837 computer models of a plasma. *J. Comput. Phys.* **14**, 148–158 (1974).

838 81. Páll, S. & Hess, B. A flexible algorithm for calculating pair interactions on  
839 SIMD architectures. *Comput. Phys. Commun.* **184**, 2641–2650 (2013).

840 82. Verlet, L. Computer ‘experiments’ on classical fluids. I. Thermodynamical  
841 properties of Lennard-Jones molecules. *Phys. Rev.* **159**, 98–103 (1967).

842 83. Tironi, I. G., Sperb, R., Smith, P. E. & Van Gunsteren, W. F. A generalized  
843 reaction field method for molecular dynamics simulations. *J. Chem. Phys.*  
844 **102**, 5451–5459 (1995).

845 84. Essmann, U. *et al.* A smooth particle mesh Ewald method. *J. Chem. Phys.*  
846 **103**, 8577–8593 (1995).

847 85. Bussi, G., Donadio, D. & Parrinello, M. Canonical sampling through  
848 velocity rescaling. *J. Chem. Phys.* **126**, 014101 (2007).

849 86. Parrinello, M. & Rahman, A. Polymorphic transitions in single crystals: A  
850 new molecular dynamics method. *J. Appl. Phys.* **52**, 7182–7190 (1981).

851 87. Abraham, M. J. *et al.* GROMACS: High performance molecular  
852 simulations through multi-level parallelism from laptops to supercomputers.  
853 *SoftwareX* **1–2**, 19–25 (2015).

854 88. Van Der Spoel, D. *et al.* GROMACS: Fast, flexible, and free. *J. Comput.*  
855 *Chem.* **26**, 1701–1718 (2005).

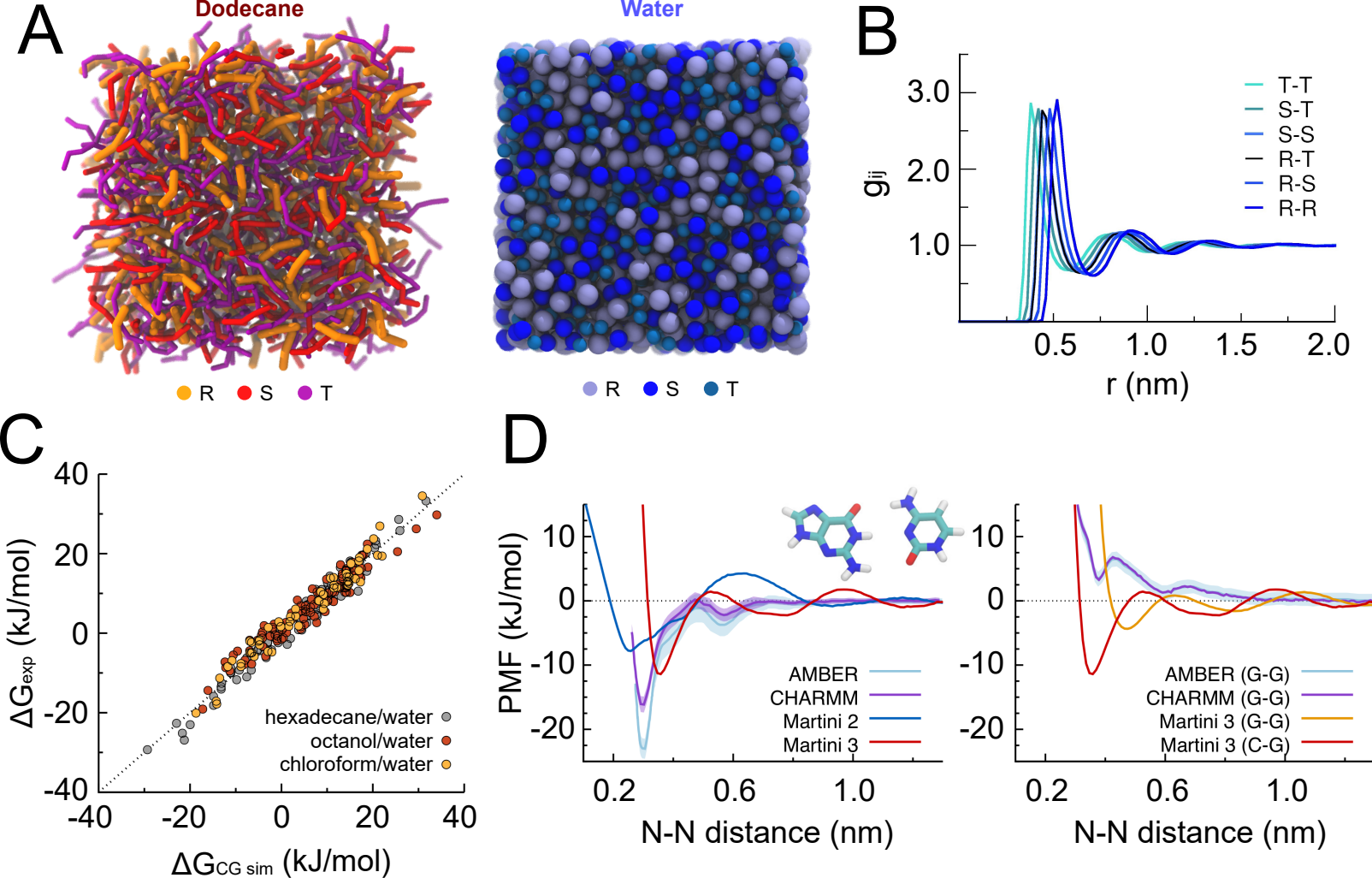
856 89. Wassenaar, T. A., Ingólfsson, H. I., Prieß, M., Marrink, S. J. & Schäfer, L.  
857 V. Mixing MARTINI: Electrostatic coupling in hybrid atomistic-coarse-grained  
858 biomolecular simulations. *J. Phys. Chem. B* **117**, 3516–3530 (2013).

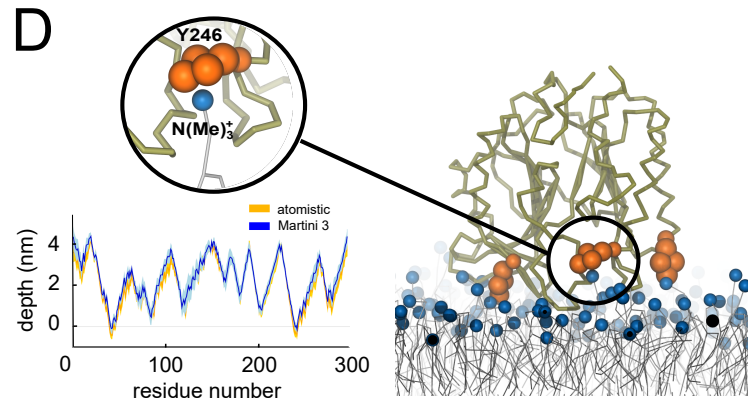
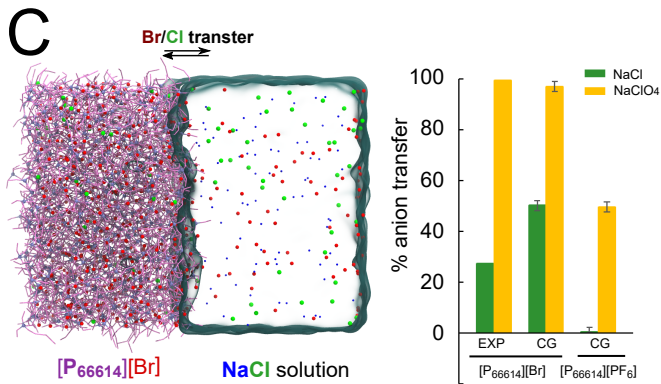
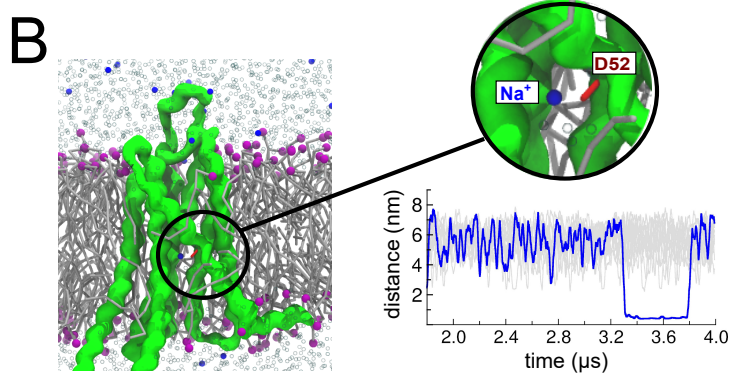
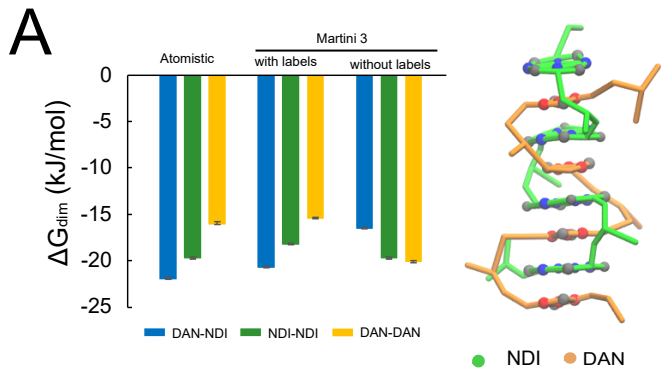
859 90. Wassenaar, T. A. *et al.* High-Throughput Simulations of Dimer and Trimer  
860 Assembly of Membrane Proteins. The DAFT Approach. *J. Chem. Theory*  
861 *Comput.* **11**, 2278–91 (2015).

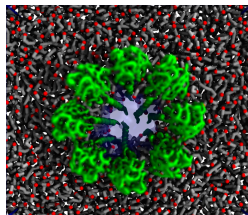
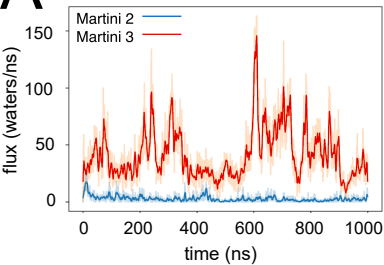
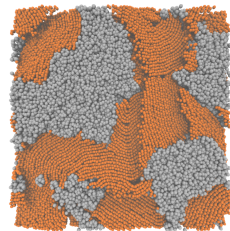
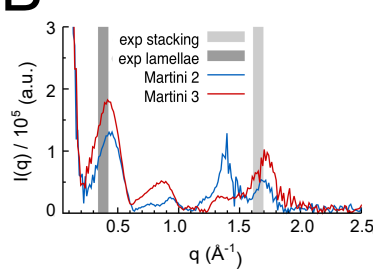
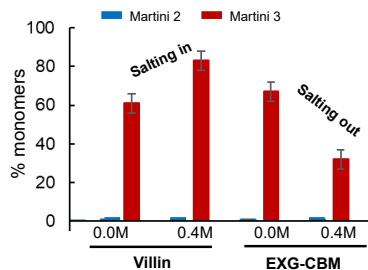
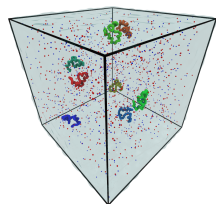
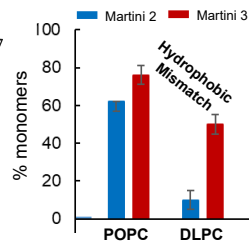
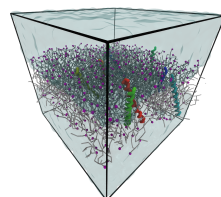
862 91. Humphrey, W., Dalke, A. and Schulten, K. VMD - Visual Molecular  
863 Dynamics. *J. Molec. Graph.* **14**, 33–38 (1996).

864 92. Gowers, R. J. *et al.* MDAnalysis: A Python Package for the Rapid Analysis  
865 of Molecular Dynamics Simulations. In *Proc. 15th Python Sci. Conference* 98–  
866 105 (2016).







**A****B****C****D****E**